DOUBLE STRATIFIED FLOW OF NANOFLUID SUBJECT TO TEMPERATURE BASED THERMAL CONDUCTIVITY AND HEAT SOURCE

by

Tasawar HAYAT[a,b], Ikram ULLAH[a*], Ahmed ALSAEDI[b], and Muhammad WAQAS[a]

[a] Department of Mathematics, Quaid-I-Azam University, Islamabad, Pakistan
[b] Non-linear Analysis and Applied Mathematics (NAAM) Research Group, Department of Mathematics, Faculty of Science, King Abdulaziz University, Jeddah, Saudi Arabia

Original scientific paper
https://doi.org/10.2298/TSCI180121242H

Stratified hydromagnetic flow of nanomaterial in the zone of stagnation point is addressed. An exponential base space dependent heat source, temperature dependent thermal conductivity and viscous dissipation are accounted. In addition, first order chemical reaction is present. The obtained non-linear system is computed by employing homotopic procedure. Convergent solutions are obtained. Plots and tabulated values are arranged for interpretation of sundry variables. Clearly temperature and concentration distributions are decayed in presence of stratification. Moreover skin friction and temperature are reduced via wall thickness parameter.

Key words: *exponential space dependent heat source, double stratification, nanomaterials, variable conductivity*

Introduction

A stratified fluid is named as the fluid with density fluctuations in the transverse direction. Density difference emerges through various sources such as pressure difference, temperature difference, and dissolved phases. The characteristics of thermal and solutal stratifications of hydrogen and oxygen in the lakes and rivers are very significant. Occurrence of wave process and smog in air-flow across the mountains are the demonstrations of the influence of stratification in atmosphere. System of thermal storage like solar ponds and heat transfer from thermal sources like condenser of power plant, rivers and seas, heat rejection from environment like lake, geothermal systems, geological transport, thermohydraulic*, etc.* are few examples of applications of stratification. Having such in view, Bansod and Jadhav [1] addressed double stratification in fluid saturated porous medium. Takhar *et al.* [2] and Chamkha [3] used different methods to explore the free convection flows. They inspected that stratification parameter reduces the temperature and skin friction. Further they found that buoyancy parameter augments the velocity and it diminishes thermal layer thickness. Double stratification in boundary-layer flow of nanoliquid by a vertical plate is discussed by Ibrahim and Makinde [4]. Hussain *et al.* [5] inspected the impact of double stratification in MHD mixed convection flow of Maxwell nanofluid. Hayat *et al.* [6] presented analysis of mixed convection in doubly stratified flow of Oldroyd-B nanofluid.

* Corresponding author, e-mail: ikram020@yahoo.com

Heat transfer liquids have remarkable role in numerous industries such as automotive industry, electronic industries*, etc.* Therefore, liquids are frequently utilized as heat transport bearer in the heat transfer apparatus. However the conventional fluids (oil, ethylene glycol, water) are poor heat conducting and usually not fulfilling the heat transfer requirement of recent industrial needs. In order to enhance their conductivity, nanometer sized particles are immersed in base fluids to form nanomaterias. By addition of such particles, thermal heat transfer properties of these liquids can be improved. It is worth to mention here that thermal conductivity, particle size, volume fraction, and temperature all participate in advancement of thermal conductivity of nanofluids. The incitement in nanofluid research streams from the heat transfer augmentation in process involving micro-manufacturing, space cooling, microchips in computer processors, fuel cells, nuclear energy, hybridpowered engines, Diesel engine oil, air refrigerators/air-conditioners and other high energy equipments. The word nanofluid was initially given by Choi [7] which refers to the liquid in which nanometer-sized (less then 100nm) disseminated. He found that addition of very less amount of nanoparticles to traditional heat transfer liquids augmented the thermal conductivity up to two times. This experimental analysis witnessed thermal conductivity enhancement of nanofluid. Buongiorno [8] further constructed a two-phas model to explore the thermal energy transport through nanoliquid. Eastman *et al.* [9] remarked that a small amount (< 1%, volume fraction) of Cu nanoparticles or CNT immersed in oil or ethylene glycol remarkably boost up the thermal conductivity of a liquid by 50% and 40%, respectively. Thus nanomaterials are recognized more significant in micro/nanoelectromechanical devices, large-scale thermal management systems through evaporators, advance cooling systems, industrial cooling applications and heat exchangers. Some other related studies of nanofluids can be seen via [10-22]. Further the magnetonanoliquids (also known as ferrofluid) are special kind of materials which are suspensions of magnetic nanoparticles like magnetite, cobalt ferrite, hematite or some other compound consisting of iron in ordinary base fluid. These particles are more useful in the sense that their physical characteristics are more tunable through the external magnetic field. Also it is worth to noted that in the absence of magnetic field these fluids behave as normal fluids. Magnetonanofluids are profitable to guide the particles up the blood stream to a tumor with magnets. It is because that magnetic nanoparticles are regarded more adhesive to tumor cells when compared with non-malignant cells. Such particles absorb more power than microparticles in alternating current magnetic fields tolerable in humans. Hyperthermia, contrast enhancement in magnetic resonance imaging, magnetic cells separation, and delivery are process where magnetonanoliquids involve. In view of such applications many scientists and engineers have interest in investigations of ferrofluids through various aspects. Stretched flow of heated ferrofluid in presence of a magnetic dipole is investigated by Andersson and Valnes [23]. Selimefendigil *et al.* [24] analyzed forced convection flow of ferrofluid. Rotating flow of magnetite water nanoliquid over a radiative stretching sheet is studied by Mustafa *et al.* [25]. Hayat *et al.* [26] examined the partial slip in flow of magnetite- Fe_3O_3 nanoparticles between rotating stretchable disks. The MHD 3-D flow of second grade nanofluid is addressed by Hayat *et al.* [27]. Sheikholeslami *et al.* [28] explained external magnetic field effect in force convection flow of nanofluid.

Present work aimed to examined combined effects of double stratification and chemical reaction in stagnation point flow of Williamson nanofluid with variable thermal conductivity. Non-linear stretching sheet of variable thickness generates the flow. Incompressible electrically conducted fluid is considered with uniform applied magnetic filed. Thermal properties of fluid are examined with viscous dissipation, Brownian motion, exponential based heat source and thermophoresis. Boundary-layer approach develops the relevant mathematical formulation.

Obtained system of equations is solved through homotopic algorithm [29-42]. Physical quantities of interest are analyzed in detail.

Mathematical development

Here we consider stagnation point flow of Williamson nanoliquid towards non-linear stretching sheet of variable thickness characterized by $y = \delta(x + b)$. Here δ characterizes that sheet is sufficiently thin. Stretching velocity of sheet is denoted by $U_w = U_0(x + b)^n$. Note that $n = 1$ corresponds to case linear stretching. A uniform magnetic field with strength B_0 is applied in transverse direction the flow. Stratification phenomenon for both heat and mass transfer are addressed. Flow analysis comprises Brownian diffusion and thermophoresis effects. Energy expression is characterize through viscous dissipation and exponential space dependent heat source. Moreover first order chemical reaction are considered. The boundary-layer problems satisfy [43-46]:

$$\frac{\partial u}{\partial x}+\frac{\partial v}{\partial y}=0 \tag{1}$$

$$u\frac{\partial u}{\partial x}+v\frac{\partial u}{\partial y}=\nu\frac{\partial^2 u}{\partial y^2}+2\nu\Gamma\frac{\partial u}{\partial y}\frac{\partial^2 u}{\partial y^2}+U_e\frac{\partial U_e}{\partial x}+\frac{\sigma B_0^2}{\rho}(U_e-u) \tag{2}$$

$$u\frac{\partial T}{\partial x}+v\frac{\partial T}{\partial y}=\frac{1}{(\rho c)_f}\frac{\partial}{\partial y}\left[k(T)\frac{\partial^2 T}{\partial y^2}\right]+\frac{(\rho c)_p}{(\rho c)_f}\left[D_B\frac{\partial T}{\partial y}\frac{\partial C}{\partial y}+\frac{D_T}{T_\infty}\left(\frac{\partial T}{\partial y}\right)^2\right]+$$
$$+\frac{\mu_0}{(\rho c)_f}\left(\frac{\partial u}{\partial y}\right)^2+\frac{\mu_0}{(\rho c)_f}\Gamma\left(\frac{\partial u}{\partial y}\right)^3+\frac{Q_0(T-T_\infty)}{(\rho c)_f}\mathrm{e}^{-n_1\xi} \tag{3}$$

$$u\frac{\partial C}{\partial x}+v\frac{\partial C}{\partial y}=D_B\frac{\partial^2 C}{\partial y^2}+\frac{D_T}{T_\infty}\frac{\partial^2 T}{\partial y^2}-k_1(C_w-C_\infty) \tag{4}$$

$$\begin{gathered}u=U_w=U_0(b+x)^n,\ v=0,\ T=T_w=T_0+d_1(b+x)\\ C=C_w=C_0+d_2(b+x)\ \text{ at }\ y=\delta(b+x)^{\frac{1-n}{2}}\end{gathered} \tag{5}$$

$$u\to U_e=U_\infty(x+b)^n,\ T\to T_\infty=T_0+e_1(b+x),\ C\to C_\infty=C_0+e_2(b+x)\ \text{as}\ y\to\infty \tag{6}$$

In previous equations the respective velocity components along (x, y) directions are represented by (u, v), $\nu = \mu_0/\rho_f$ the kinematic viscosity, b, d_1, d_2, e_1, and e_2 are the dimensional constants, Q_0 – the heat source parameter, μ_0 – the dynamic viscosity, n_1 – the exponential index, ρ_f – the base liquid density, U_e – the free stream velocity, Γ – the time constant, n – the velocity power index, σ – the electrical conductivity, T – the temperature, T_0 – the reference temperature, $(\rho c)_f$ – the heat capacity of liquid, $(\rho c)_p$, – the nanoparticles effective heat capacity, k_1 – the chemical reaction rate, D_B – the diffusion coefficient, C_0 – the reference concentration, C – the concentration, D_T – the coefficient of thermophoretic diffusion, T_∞ and C_∞ the ambient liquid temperature and concentration, respectively and U_0 the reference velocity. Consider the variable thermal conductivity in the form [47]:

$$k(T)=k_\infty\left[1+\varepsilon\frac{T-T_\infty}{\Delta T}\right] \tag{7}$$

where $\Delta T = T_w - T_0$ and k_∞ is the ambient conductivity. With the help of following transformations:

$$u = U_0(x+b)^n F'(\eta),\ v = -\sqrt{\left(\frac{n+1}{2}\right)\nu U_0(x+b)^{n-1}}\left[F(\eta)+\eta F'(\eta)\left(\frac{n-1}{n+1}\right)\right]$$
$$\eta = y\sqrt{\left(\frac{n+1}{2}\right)\frac{U_0(x+b)^{n-1}}{\nu}}\ \Theta(\eta) = \frac{T-T_\infty}{T_w-T_0},\ \Phi(\eta) = \frac{C-C_\infty}{C_w-C_0} \tag{8}$$

equation (1) is trivially verified while eqs. (2)-(7) yield:

$$F''' + FF'' - \left(\frac{2n}{n+1}\right)F'^2 + \mathrm{We}\sqrt{\frac{n+1}{2}}F''F''' + \left(\frac{2}{n+1}\right)M^2(\lambda - F') + \left(\frac{2n}{n+1}\right)\lambda^2 = 0 \tag{9}$$

$$(1+\varepsilon\Theta)\Theta'' + \varepsilon\Theta' + \mathrm{Pr}\left[F\Theta' + Nb\Theta'\Phi' + Nt\Theta'^2 - \tfrac{2}{n+1}(\varepsilon_1+\Theta)F'\right] +$$
$$+ \mathrm{We}\,\mathrm{Pr}\,\mathrm{Ec}F''^3 + \mathrm{Pr}\,\mathrm{Ec}F''^2 + \left(\frac{2}{n+1}\right)\mathrm{Pr}\,Q\exp(-n_1\xi)\Theta = 0 \tag{10}$$

$$\Phi'' + \mathrm{Sc}\left(F\Phi' - \frac{2}{n+1}\varepsilon_2 F'\right) + \left(\frac{Nt}{Nb}\right)\Theta'' - \left(\frac{2}{n+1}\right)\mathrm{Sc}\gamma_1\Phi = 0 \tag{11}$$

$$F(\alpha) = \alpha\left(\frac{1-n}{1+n}\right),\ F'(\alpha) = 1,\ F'(\infty)\to\lambda$$
$$\Theta(\alpha) = 1-\varepsilon_1,\ \Theta(\infty)\to 0 \tag{12}$$
$$\Phi(\alpha) = 1-\varepsilon_2,\ \Phi(\infty)\to 0$$

In previous expressions prime signifies derivative with respect to η and

$$\alpha = \delta\sqrt{\left(\frac{n+1}{2}\right)\frac{U_0}{\nu}}$$

designates wall thickness parameter and

$$\alpha = \eta = \delta\sqrt{\left(\frac{n+1}{2}\right)\frac{U_0}{\nu}}$$

Considering the following expression $F(\eta) = f(\eta - \alpha) = f(\xi)$, $\Theta(\eta) = \theta(\eta - \alpha) = \theta(\xi)$, and $\Phi(\eta - \alpha) = \phi(\eta - \alpha) = \phi(\xi)$, eqs. (9)-(12) become:

$$f''' + ff'' - \left(\frac{2n}{n+1}\right)f'^2 + \mathrm{We}\sqrt{\frac{n+1}{2}}f''f''' + \left(\frac{2}{n+1}\right)M^2(\lambda - f') + \left(\frac{2n}{n+1}\right)\lambda^2 = 0 \tag{13}$$

$$(1+\varepsilon\theta)\theta'' + \varepsilon\theta' + \mathrm{Pr}\left[f\theta' + Nb\theta'\phi' + Nt\theta'^2 - \frac{2}{n+1}(\varepsilon_1+\theta)f'\right] +$$
$$+ \mathrm{We}\,\mathrm{Pr}\,\mathrm{Ec}f''^3 + \mathrm{Pr}\,\mathrm{Ec}f''^2 + \left(\frac{2}{n+1}\right)\mathrm{Pr}\,Q\exp(-n_1\xi)\theta = 0 \tag{14}$$

$$\phi'' + \mathrm{Sc}\left(f\phi' - \frac{2}{n+1}\varepsilon_2 f'\right) + \left(\frac{Nt}{Nb}\right)\theta'' - \frac{2}{n+1}\mathrm{Sc}\gamma_1\phi = 0 \tag{15}$$

$$\begin{gathered} f(0) = \alpha\left(\frac{1-n}{1+n}\right),\ f'(0) = 1,\ f'(\infty) \to \lambda \\ \theta(0) = 1-\varepsilon_1,\ \ \theta(\infty) \to 0 \\ \phi(0) = 1-\varepsilon_2,\ \ \phi(\infty) \to 0 \end{gathered} \tag{16}$$

where We is the shows Weissenberg number, Q – the exponential space based heat source (ESHS) parameter, Ec – the Eckert number, Pr – the Prandtl number, λ – the for the ratio of velocities, M – the magnetic parameter, Nt – the thermophoresis parameter, Nb – the Brownian motion parameter, γ_1 – the for chemical reaction, Sc – the for Schmidt number, ε_1 – the for thermal stratified parameter, ε – the for variable thermal conductivity, and ε_2 – the solutal stratified parameter. The non-dimensional quantities are defined:

$$\begin{gathered} \mathrm{We} = \Gamma\sqrt{\frac{(n+1)U_0^3(x+b)^{3n-1}}{\nu}},\ \lambda = \frac{U_\infty}{U_0},\ \mathrm{Ec} = \frac{U_w^2}{c_p(T_w - T_0)},\ \mathrm{Pr} = \frac{\mu c_p}{k_\infty} \\ \varepsilon_1 = \frac{e_1}{d_1},\ \varepsilon_2 = \frac{e_2}{d_2},\ \gamma_1 = \frac{k_1}{U_0}(x+b)^{1-n},\ M^2 = \frac{\sigma B_0^2}{\rho U_0 (x+b)^{n-1}} \\ Q = \frac{Q_0}{(\rho c)_f U_0 (x+b)^{n-1}},\ \mathrm{Sc} = \frac{\nu}{D_B},\ Nb = \frac{(\rho c)_p}{(\rho c)_f}\frac{D_B(C_w - C_0)}{\nu},\ Nt = \frac{(\rho c)_p}{(\rho c)_f}\frac{D_T(T_w - T_0)}{T_\infty \nu} \end{gathered} \tag{17}$$

Expressions of skin friction and rates of heat and mass transfer rates at the surface:

$$C_{fx} = \frac{\tau_{yx}\,|_{y=\delta(b+x)^{\frac{1-n}{2}}}}{1/2\rho U_w^2} = \frac{\mu_0\left[\dfrac{\partial u}{\partial y} + \dfrac{\Gamma}{2}\left(\dfrac{\partial u}{\partial y}\right)\right]_{y=\delta(x+b)^{\frac{1-n}{2}}}}{\rho U_w^2} \tag{18}$$

$$\mathrm{Nu}_x = \frac{(x+b)q_w\,|_{y=\delta(b+x)^{\frac{1-n}{2}}}}{k_\infty(T_w - T_\infty)} = -\frac{\left(\dfrac{\partial T}{\partial y}\right)_{y=\delta(x+b)^{\frac{1-n}{2}}}}{T_w - T_\infty} \tag{19}$$

$$\mathrm{Sh}_x = \frac{(x+b)q_m\,|_{y=\delta(b+x)^{\frac{1-n}{2}}}}{D_B(C_w - C_\infty)} = -\frac{\left(\dfrac{\partial C}{\partial y}\right)_{y=\delta(x+b)^{\frac{1-n}{2}}}}{C_w - C_\infty} \tag{20}$$

In dimensionless form we have:

$$\left(\mathrm{Re}_x\right)^{0.5} C_{f_x} = \sqrt{\frac{(n+1)}{2}} f''(0) + \left(\frac{n+1}{4}\right)\mathrm{We} f''^2(0) \tag{21}$$

$$\left(\mathrm{Re}_x\right)^{-0.5}\mathrm{Nu}_x = -\sqrt{\left(\frac{n+1}{2}\right)}\theta'(0) \tag{22}$$

$$\left(\mathrm{Re}_x\right)^{-0.5}\mathrm{Sh}_x = -\sqrt{\left(\frac{n+1}{2}\right)}\phi'(0) \tag{23}$$

where $\mathrm{Re}_x = U_w(b+x)/\nu$ depicts the local Reynolds number.

Homotopic solutions and convergence analysis

The initial approximations (f_0, θ_0, ϕ_0) and linear operators ($\bar{\mathbf{L}}_f$, $\bar{\mathbf{L}}_\theta$, $\bar{\mathbf{L}}_\phi$) are defined:

$$\begin{aligned} f_0(\xi) &= \alpha\left(\frac{1-n}{1+n}\right) + (1-\lambda)\left(1-\mathrm{e}^{-\xi}\right) + \lambda\xi \\ \theta_0(\xi) &= (1-\varepsilon_1)\mathrm{e}^{-\xi} \\ \phi_0(\xi) &= (1-\varepsilon_2)\mathrm{e}^{-\xi} \end{aligned} \tag{24}$$

with

$$\begin{aligned} \bar{\mathbf{L}}_f\left[\beta_1^{**} + \beta_2^{**}\mathrm{e}^{\xi} + \beta_3^{**}\mathrm{e}^{-\xi}\right] &= 0 \\ \bar{\mathbf{L}}_\theta\left[\beta_4^{**}\mathrm{e}^{\xi} + \beta_5^{**}\mathrm{e}^{-\xi}\right] &= 0 \\ \bar{\mathbf{L}}_\phi\left[\beta_6^{**}\mathrm{e}^{\xi} + \beta_7^{**}\mathrm{e}^{-\xi}\right] &= 0 \end{aligned} \tag{25}$$

in which β_j^{**} (j = 1-7) depict the arbitrary constants:

$$(1-\tilde{p})\mathbf{L}_f\left[\hat{f}(\xi,\tilde{p}) - f_0(\xi)\right] = \tilde{p}\hbar_f\mathbf{N}_f\left[\hat{f}(\xi,\tilde{p})\right] \tag{26}$$

$$(1-\tilde{p})\mathbf{L}_\theta\left[\hat{\theta}(\xi,\tilde{p}) - \theta_0(\xi)\right] = \tilde{p}\hbar_\theta\mathbf{N}_\theta\left[\hat{f}(\xi,\tilde{p}), \hat{\theta}(\xi,\tilde{p}), \hat{\phi}(\xi,\tilde{p})\right] \tag{27}$$

$$(1-\tilde{p})\mathbf{L}_\phi\left[\hat{\phi}(\xi,\tilde{p}) - \phi_0(\xi)\right] = \tilde{p}\hbar_\phi\mathbf{N}_\phi\left[\hat{f}(\xi,\tilde{p}), \hat{\theta}(\xi,\tilde{p}), \hat{\phi}(\xi,\tilde{p})\right] \tag{28}$$

$$\begin{aligned} \hat{f}(0,\tilde{p}) &= \alpha\left(\frac{1-n}{1+n}\right),\ \hat{f}'(0,\tilde{p}) = 1,\ \hat{f}'(\infty,\tilde{p}) = 0 \\ \hat{\theta}(0,\tilde{p}) &= (1-\varepsilon_1),\ \hat{\theta}(\infty,\tilde{p}) = 0 \\ \hat{\phi}(0,\tilde{p}) &= (1-\varepsilon_1),\ \hat{\phi}(\infty,\tilde{p}) = 0 \end{aligned} \tag{29}$$

$$\begin{aligned} \mathbf{N}_f\left[\hat{f}(\xi;\tilde{p})\right] = \frac{\partial^3\hat{f}}{\partial\xi^3} + \frac{\partial^2\hat{f}}{\partial\xi^2}\hat{f} - \frac{2n}{n+1}\left(\frac{\partial\hat{f}}{\partial\xi}\right)^2 + \mathrm{We}\sqrt{\frac{n+1}{2}}\frac{\partial^2\hat{f}}{\partial\xi^2}\frac{\partial^3\hat{f}}{\partial\xi^3} + \\ + \frac{2}{n+1}\mathrm{M}^2\left(\lambda - \frac{\partial\hat{f}}{\partial\xi}\right) + \frac{2n}{n+1}\lambda^2 \end{aligned} \tag{30}$$

$$\mathbf{N}_\theta\left[\hat{\theta}(\xi,\tilde{p}),\hat{\phi}(\xi,\tilde{p}),\hat{f}(\xi;\tilde{p})\right]=\left(1+\varepsilon\hat{\theta}\right)\frac{\partial^2\hat{\theta}}{\partial\xi^2}+\varepsilon\hat{\theta}'+\Pr\hat{f}\frac{\partial\hat{\theta}}{\partial\xi}+\Pr Nb\frac{\partial\hat{\theta}}{\partial\xi}\frac{\partial\hat{\phi}}{\partial\xi}+$$
$$+\Pr Nt\left(\frac{\partial\hat{\theta}}{\partial\xi}\right)^2-\Pr\frac{2}{n+1}(\varepsilon_1+\hat{\theta})\frac{\partial\hat{f}}{\partial\xi}+\mathrm{WePrEc}\left(\frac{\partial\hat{f}}{\partial\xi}\right)^3+\Pr\mathrm{Ec}\left(\frac{\partial\hat{f}}{\partial\xi}\right)^2+\left(\frac{2}{n+1}\right)\Pr Q\exp(-n_1\xi)\hat{\theta} \quad (31)$$

$$\mathbf{N}_\phi[\hat{\phi}(\xi,\tilde{p}),\hat{\theta}(\xi,\tilde{p}),\hat{f}(\xi;\tilde{p})]=\frac{\partial^2\hat{\phi}}{\partial\xi^2}+\mathrm{Sc}\hat{f}\frac{\partial\hat{\phi}}{\partial\xi}+\frac{Nt}{Nb}\frac{\partial^2\hat{\theta}}{\partial\xi^2}-$$
$$-\mathrm{Sc}\varepsilon_2\frac{2}{n+1}\frac{\partial\hat{f}}{\partial\xi}-\frac{2}{n+1}\mathrm{Sc}\gamma_1\hat{\phi} \quad (32)$$

$$\mathbf{L}_f\left[f_m(\xi)-\chi_m f_{m-1}(\xi)\right]=\hbar_f\mathbf{R}_f^m(\xi) \quad (33)$$

$$\mathbf{L}_\theta\left[\theta_m(\xi)-\chi_m\theta_{m-1}(\xi)\right]=\hbar_\theta\mathbf{R}_\theta^m(\xi) \quad (34)$$

$$\mathbf{L}_\phi\left[\phi_m(\xi)-\chi_m\phi_{m-1}(\xi)\right]=\hbar_\phi\mathbf{R}_\phi^m(\xi) \quad (35)$$

$$\begin{gathered}f_m(0)=f_m'(0)=f_m'(\infty)=0,\ \theta_m(0)=0\\ \theta_m(\infty)=0,\ \phi_m(0)=0,\ \phi_m(\infty)=0\end{gathered} \quad (36)$$

$$\mathbf{R}_f^m(\xi)=f_{m-1}'''(\xi)+\sum_{k=0}^{m-1}f_{m-1-k}f_k''-\frac{2n}{n+1}\sum_{k=0}^{m-1}f_{m-1-k}'f_k'+$$
$$+\mathrm{We}\sqrt{\frac{n+1}{2}}\sum_{k=0}^{m-1}f_{m-1-k}f_k'''\frac{2}{n+1}M^2(1-\chi_m)-\frac{2}{n+1}M^2f_{m-1}+\frac{2n}{n+1}\lambda(1-\chi_m) \quad (37)$$

$$\mathbf{R}_\theta^m(\xi)=[1+\varepsilon\theta_{m-1}(\xi)]\theta_{m-1}''(\xi)+\varepsilon\theta_{m-1}'(\xi)+\Pr\sum_{k=0}^{m-1}f_{m-1-k}\theta_k'+\Pr Nb\sum_{k=0}^{m-1}f_{m-1-k}'\theta_k'+$$
$$+\Pr Nt\sum_{k=0}^{m-1}\theta_{m-1-k}'\theta_k'-\tfrac{2}{n+1}\Pr\varepsilon_1f_{m-1}'(\xi)-\tfrac{2}{n+1}\Pr\sum_{k=0}^{m-1}f_{m-1-k}\theta_k+$$
$$+\mathrm{We}\Pr\mathrm{Ec}f_{m-1}''(\xi)\sum_{k=0}^{m-1}f_{m-1-k}''\sum_{l=0}^{k}f_{k-l}''f_l''+\Pr\mathrm{Ec}\sum_{k=0}^{m-1}f_{m-1-k}''f_k''+\left(\frac{2}{n+1}\right)\Pr Q\exp(-n_1\xi)\theta_{m-1}(\xi) \quad (38)$$

$$\mathbf{R}_\phi^m(\xi)=\phi_{m-1}''(\xi)+\mathrm{Sc}\sum_{k=0}^{m-1}f_{m-1-k}\phi_k'+\left(\frac{Nt}{Nb}\right)\theta_{m-1}''(\xi)-\frac{2}{n+1}\varepsilon_2f_{m-1}'(\xi)-\frac{2}{n+1}\mathrm{Sc}\gamma_1\phi_{m-1}(\xi) \quad (39)$$

$$\chi_m=\begin{cases}0, & m\le 1\\ 1, & m>1\end{cases} \quad (40)$$

The general solutions, $f_m(\xi)$, $\theta_m(\xi)$, $\phi_m(\xi)$, of the governing in the form of special solutions, $f_m^*(\xi)$, $\theta_m^*(\xi)$, $\phi_m^*(\xi)$:

$$f_m(\xi) = f_m^*(\xi) + \beta_1^{**} + \beta_2^{**}e^{\xi} + \beta_3^{**}e^{-\xi} \tag{41}$$

$$\theta_m(\xi) = \theta_m^*(\xi) + \beta_4^{**}e^{\xi} + \beta_5^{**}e^{-\xi} \tag{42}$$

$$\phi_m(\xi) = \phi_m^*(\xi) + \beta_6^{**}e^{\xi} + \beta_7^{**}e^{-\xi} \tag{43}$$

Obviously homotopic procedure for local similar solutions involves embedding variables which gives the flexibility to enlarge the convergence region. Thus $\hbar$-curves are displayed which enable us to find the acceptable values of $\hbar_f$, $\hbar_\theta$, and $\hbar_\phi$, figs. 1 and 2. Allowed ranges of $\hbar_f$, $\hbar_\theta$, and $\hbar_\phi$ are $[-1.10 \leq \hbar_f \leq -2.00]$, $[-0.40 \leq \hbar_\theta \leq -1.40]$, and $[-0.50 \leq \hbar_\phi \leq -1.63]$. Further homotropy analysis method solutions converge when $\hbar_f = -5.0 = \hbar_\theta$ and $\hbar_\phi = -0.6$, see tab. 1.

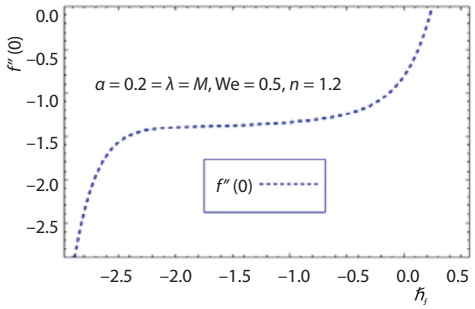

Figure 1. The $\hbar$-curves for $f(\xi)$

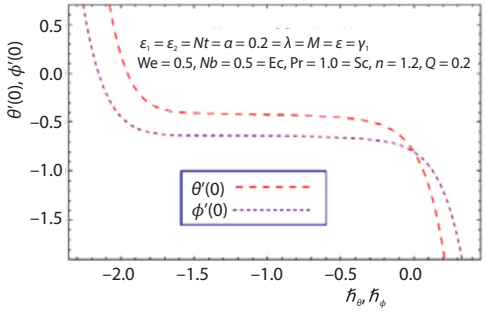

Figure 2. The $\hbar$-curves for $\theta(\xi)$ and $\phi(\xi)$

Table 1. Convergence of solutions when Ec = *Nb* = We, *Q* = *M* = *α* = 0.2 = *n* = *λ* = *ε* = ε_1 = ε_2 = *Nt* = γ_1, and Pr = 1.0 = Sc

Order of estimations	$-f''(0)$	$\theta'(0)$	$\phi'(0)$
1	0.88582	0.88582	0.75752
10	1.21754	1.21754	0.65816
15	1.28024	1.28024	0.64700
20	1.32201	1.32201	0.64057
25	1.33218	1.33218	0.63923
30	1.33218	1.33218	0.63912
40	1.33218	1.33218	0.63911

Discussion

The transformed problems defined in eqs. (13)-(16) is solved analytically via homotopic technique. Influence of some sundry variables like Weissenberg number, velocities ratio parameter, λ, (ESHS) parameter, Q, magnetic parameter, M, variable thermal conductivity parameter, ε, velocity power index, n, Prandtl number, thermophoresis parameter, Nt, Eckert number, Brownian motion parameter, Nb, thermal stratified parameter, ε_1, solutal stratified parameter, ε_2, Schmidt number, chemical reaction, γ_1, and wall thickness parame-

ter, α, velocity, temperature, concentration, local Nusselt and Sherwood numbers. For such intention figs. 3-22 have been interperted. The role of wall thickness parameter α on $f'(\xi)$ is depicted in figs. 3 and 4. It is noted here that $f'(\xi)$ near the plate decays as α increases for $n > 1$, see fig. 3, and opposite trend is seen for $n < 1$, see fig. 4. Graphical presentation for velocity field as a function of n is elucidated through fig. 5. It appears that larger n cause to enhanced the stretching velocity which accelerates the fluid motion and consequently the fluid velocity increases. Thickness of momentum layer becomes thin as n increases. Impact of We on $f'(\xi)$ is presented in fig. 6. In physical sense, We increases the fluid thickness and consequently velocity profile $f'(\xi)$ decays. Behavior of λ on $f'(\xi)$ is disclosed via fig. 7. It is examined that velocity enhances with increment in λ. Thickness of momentum layer increases for $A < 1$. Here stretching velocity dominates the free stream velocity. Variation in $\theta(\xi)$ via ε is examined in fig. 8. Here increment in ε boosts up liquid temperature significantly. Figure 9 is portrayed to see the changes in Nt for $\theta(\xi)$. It is noticed that when we strengthen Nt from $Nt = 0.2$ to $Nt = 0.1$, it sharply rises $\theta(\xi)$ and thermal layer thickness. More precisely we can say that thermophoresis force has the property that nanoparticles near the hot surface are being pushed towards the cold region at the boundary. Thus in presence of Nt one can expects thermal layer to become thicker. Feature of Pr on $\theta(\xi)$ is portrayed in fig. 10. Reduction in $\theta(\xi)$ is noticed for higher Pr. By increasing Pr the thermal diffusivity diminishes because heat rapidly transfers that causes a drop in temperature distribution. Analysis for behavior of Ec is depicted in fig. 11. It is concluded that $\theta(\xi)$ is an increasing function of Ec. Physically frictional heating is associated with higher Ec thus have $\theta(\xi)$ increases. Effects of wall thickness parameter α on $\theta(\xi)$ is illustrated in fig. 12. It is concluded that $\theta(\xi)$ is decaying function of α. In fact significant amount of heat transferred from surface to fluid when α is incriminated. Figure 13 displays characteristics of ε_1 on $\theta(\xi)$. Clearly

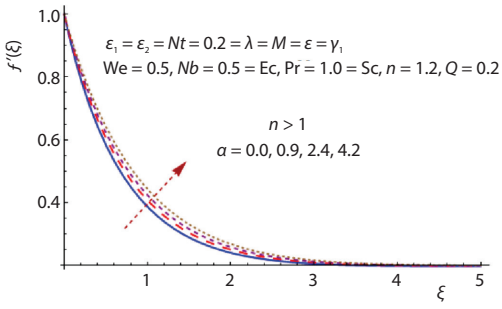

Figure 3. Impact of $f'(\xi)$ via α ($n > 1$)

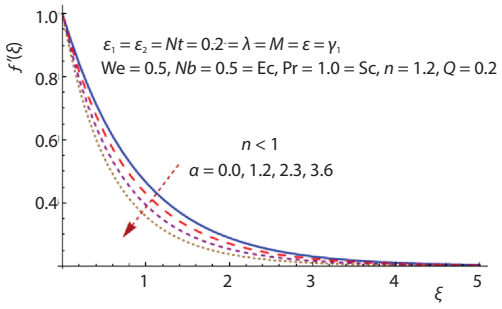

Figure 4. Impact of $f'(\xi)$ via α ($n < 1$)

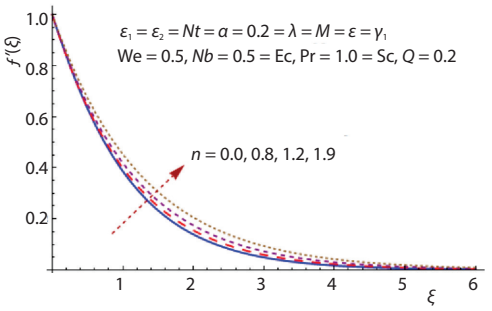

Figure 5. Impact of $f'(\xi)$ via n

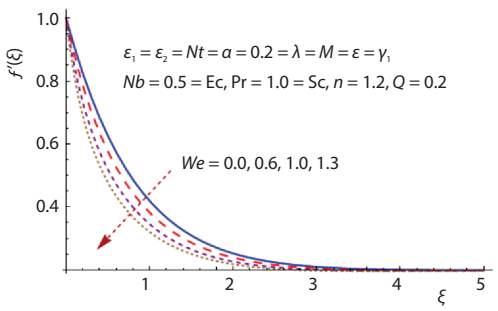

Figure 6. Impact of $f'(\xi)$ via We

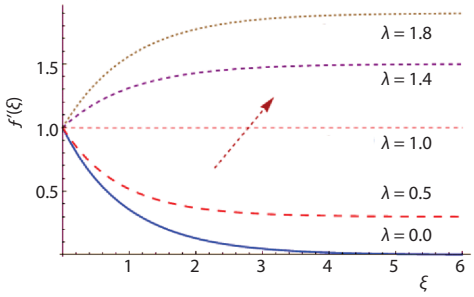

Figure 7. Impact of $f'(\xi)$ via λ

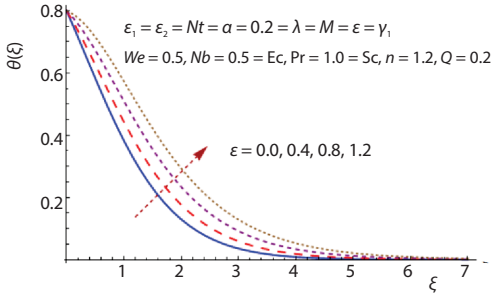

Figure 8. Impact of $\theta(\xi)$ via ε

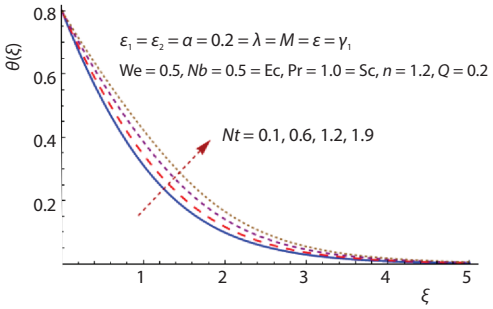

Figure 9. Impact of $\theta(\xi)$ via Nt

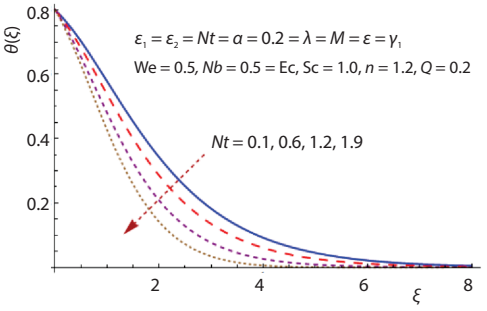

Figure 10. Impact of $\theta(\xi)$ via Pr

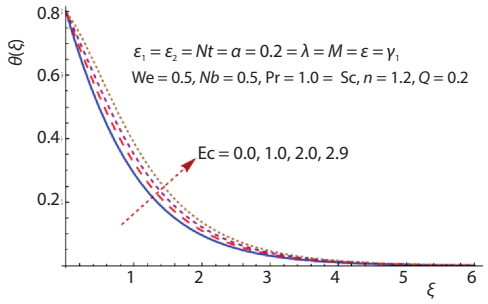

Figure 11. Impact of $\theta(\xi)$ via Ec

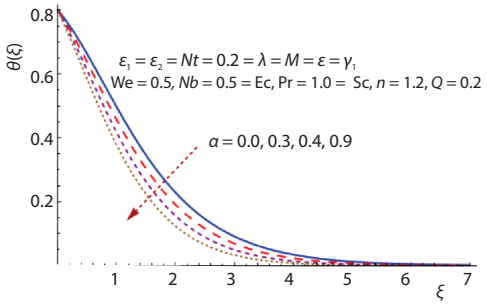

Figure 12. Impact of $\theta(\xi)$ via α

$\theta(\xi)$ reduces for larger thermal stratification parameter. It is because of the fact that temperature difference slowly decays between the sheet and ambient liquid. Temperature is an increasing function of Q, see fig. 14. Influence of Nt on $\phi(\xi)$ is drawn in fig. 15. Here $\phi(\xi)$ is higher for Nt. Salient feature of Nb on nanoparticles concentration $\phi(\xi)$ is declared in fig. 16. For larger Nb a decreasing trend of $\phi(\xi)$ is noticed. Concentration distribution is reduced via Sc, see fig. 17. Figure 18 shows effects of ε_2 on $\phi(\xi)$. It is reveled that $\phi(\xi)$ decreases via ε_2. This is due to small difference of surface and ambient concentration. Role of γ_1 on $\phi(\xi)$ is captured in fig. 19. Clearly stronger γ_1 lead to reduce $\phi(\xi)$ and solutal boundary-layer thickness. Figure 20 shows Nb and Nt variations for Nusselt number. It is found that heat transfer rate diminishes for larger Nb while it increases via Nt. Figure 21 shows that Nusselt number for higher M while reverse is seen for

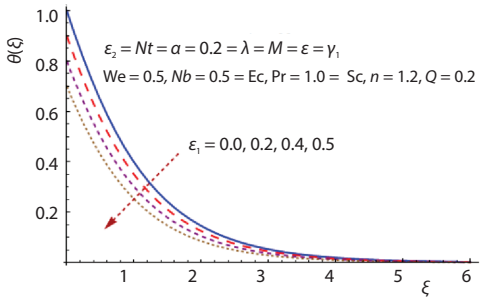

Figure 13. Impact of $\theta(\xi)$ via ε_1

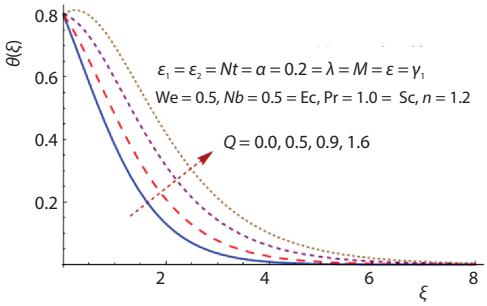

Figure 14. Impact of $\theta(\xi)$ via Q

larger n. It is noticed that Nusselt number increases with increasing M. Variations of n and Sc on Sherwood number ($\mathrm{Sh}_x \mathrm{Re}_x^{-0.5}$) are portrayed in fig. 22. Clearly $\mathrm{Sh}_x \mathrm{Re}_x^{-0.5}$ boosts up for higher values of Sc and n. Numerical data of $-f''(0)$, $\theta'(0)$, and $\phi'(0)$ for various order of estimations are demonstrated in tab. 1 when $Q = M = \alpha = 0.2 = n = \lambda = \varepsilon = \varepsilon_1 = \varepsilon_2 = Nt = \gamma_1$, $\mathrm{Ec} = Nb = 0.5 = \mathrm{We}$, $\mathrm{Pr} = 1.0 = \mathrm{Sc}$, and $\hbar_f = \hbar_\theta = -0.4 = \hbar_\phi$. It is depicted that 30$^{\text{th}}$ order of estimations are enough for convergence of homotopic solutions. Numerical results of skin friction coefficient $-(\mathrm{Re})^{1/2} C_{fx}$ for various values of λ, We, M, n, and α are presented in tab. 2. Here skin friction coefficient is enhanced via λ, We, M, n, and α.

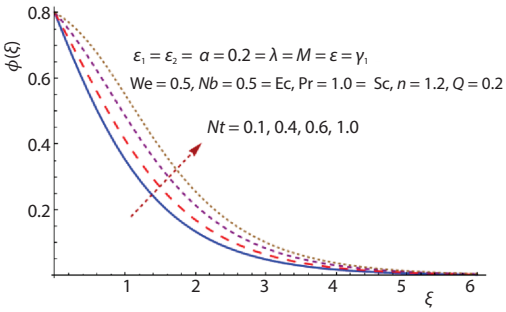

Figure 15. Impact of $\phi(\xi)$ via Nt

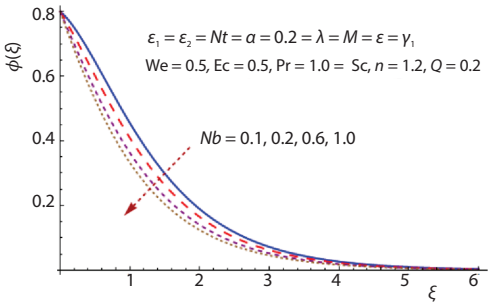

Figure 16. Impact of $\phi(\xi)$ via Nb

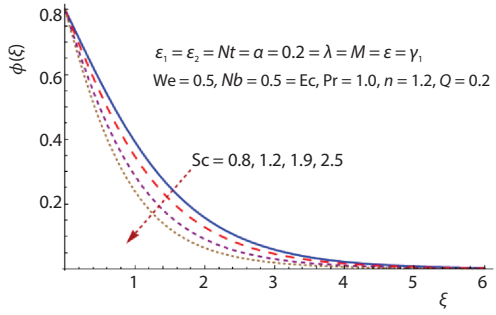

Figure 17. Impact of $\phi(\xi)$ via Sc

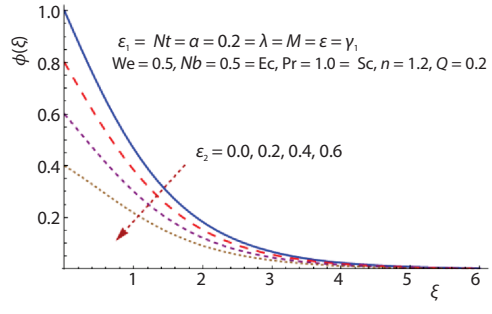

Figure 18. Impact of $\phi(\xi)$ via ε_2

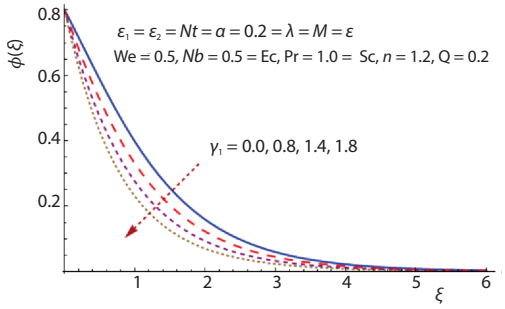

Figure 19. Impact of $\phi(\xi)$ via γ_1

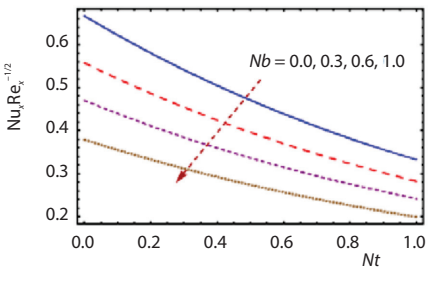

Figure 20. Impact of *Nb* via *Nt* on $Nu_x Re_x^{-1/2}$

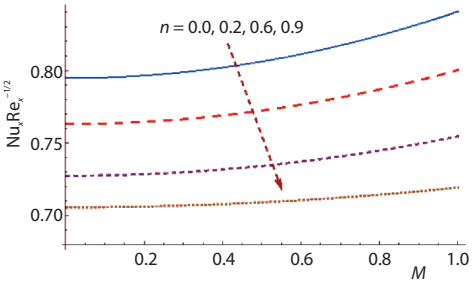

Figure 21. Impact of *n* via *M* on $Nu_x Re_x^{-1/2}$

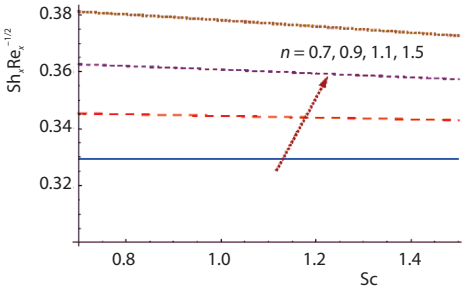

Figure 22. Impact of *n* via Sc on $Sh_x Re_x^{-1/2}$

Table 2. Computation for numerical data of surface drag force $-(Re)^{1/2} C_{fx}$ for distinct values of We, *M*, *n*, λ, and α

Parameters (fixed values)	Parameters		$-(Re)^{1/2} C_{fx}$
$Q = \alpha = 0.2 = n = \lambda = \varepsilon = \varepsilon_1 = \varepsilon_2 = Nt = \gamma_1$	M	0.0	0.930131
Ec = Nb = 0.5 = We, Pr = 1.0 = Sc		0.3	0.946343
		0.6	0.983631
$Q = M = \alpha = 0.2 = n = \lambda = \varepsilon = \varepsilon_1 = \varepsilon_2 = Nt = \gamma_1$	We	0.0	1.94118
Ec = Nb = 0.5 = We, Pr = 1.0 = Sc		0.4	1.245294
		0.8	0.478471
$Q = M = \alpha = 0.2 = \lambda = \varepsilon = \varepsilon_1 = \varepsilon_2 = Nt = \gamma_1$	n	0.5	0.865803
Ec = Nb = 0.5 = We, Pr = 1.0 = Sc		1.0	0.961150
		1.5	0.975210
$Q = M = 0.2 = n = \lambda = \varepsilon = \varepsilon_1 = \varepsilon_2 = Nt = \gamma_1$	α	0.2	0.951138
Ec = Nb = 0.5 = We, Pr = 1.0 = Sc		0.6	0.938785
		0.8	0.928758
$Q = M = \alpha = 0.2 = n = \varepsilon = \varepsilon_1 = \varepsilon_2 = Nt = \gamma_1$	λ	0.2	0.930158
Ec = Nb = 0.5 = We, Pr = 1.0 = Sc		0.5	0.887362
		0.8	0.125043

Conclusions

Main observations of carried out analysis are outlined as follows.

- Wall thickness parameter α decreases both velocity and temperature.
- Increment in Weissenberg number reduces the velocity field.
- Both ε_1 and ε_2 have similar effects on temperature and concentration.
- Higher values of ε augment fluid temperature.
- Temperature and concentration show increasing behavior when *Nt* is enhanced.
- Skin friction reduces for higher *n*.
- Features of *Nt* and *Nb* on Nusselt number are quite reverse.

Nomenclature

b, d_1, d_2, e_1, e_2 – dimensional constants
C_{fx} – skin friction
C, C_w – nanoparticles and wall concentrations
C_∞, C_0 – ambient and reference concentrations
D_B, D_T – coefficients of Brownian and themophoretic diffusion
Ec – Eckert number
F, f' – dimensionless velocities
k_1 – chemical reaction rate
k_∞ – ambient thermal conductivity
M – magnetic parameter
Nb – Brownian motion parameter
Nt – thermopherasis parameter
Nu – Nusselt number
n – velocity power index
n_1 – exponential index
Pr – Prandtl number
Q – the ESHS parameter
Q_0 – heat source parameter
Re_x – local Reynolds number
Sc – Schmidt number
Sh_x – Sherwood number
T_w, T – wall and liquid temperatures
T_∞, T_0 – ambient and reference temperatures
U_e – free stream velocity
U_w, U_0 – stretching and reference velocities
u, v – velocity components
x, y – Cartesian co-ordinates
We – Weissenberg number

Greek symbols

α – wall thickness parameter
Γ – time constant
γ_1 – chemical reaction parameter
δ – small parameter regarding the surface sufficiently thin
ε – variable thermal conductivity parameter
ε_1, ε_2 – thermal and solutal stratified parameters
Θ, θ – dimensionless temperatures
λ – ratio of velocities
μ_0 – dynamic viscosity
ν – kinematic viscosity
ρ – fluid density
$(\rho c)_f$ – nanoparticles effective capacity
$(\rho c)_p$ – heat capacity of liquid
σ – electrical conductivity
Φ, ϕ – dimensionless concentration

References

[1] Bansod, V., Jadhav, R., Effect of Double Stratification on Mixed Convection Heat and Mass Transfer from a Vertical Surface in a Fluid-Saturated Porous Medium, *Heat Transfer Asian Research*, *39* (2010), 6, pp. 378-395
[2] Takhar, H. S., *et al*., Natural-Convection Flow from a Continously Moving Vertical Surface Immersed in a Thermally Stratified Medium, *Heat Mass transfer*, *38* (2001), Nov., pp. 17-24
[3] Chamkha, A. J., Hydromahnetic Natural-Convection from an Isothermal Inclined Surface Adjacent to a Thermally Stratified Porous Medium, *International Journal of Engineering Science*, *35* (1997), 10-11, pp. 975-986
[4] Ibrahim, W., Makinde, O. D., The Effect of Double Stratification on Boundary-Layer Flow and Heat Transfer of Nanofluid over a Vertical Plate, *Computers and Fluids*, *86* (2013), Nov., pp. 433-441
[5] Hussain, T., *et al*., Impact of Double Stratification and Magnetic Field in Mixed Convective Radiative flow of Maxwell Nanofluid, *Journal of Molecular Liquids*, *220* (2016), Aug., pp. 870-878
[6] Hayat, T., *et al*., Thermal and Solutal Stratification in Mixed Convection 3-D flow of an Oldroyd-B Nanofluid, *Results in Physics*, *7* (2017), Oct., pp. 3797-3805
[7] Choi, S. U. S., Enhancing Thermal Conductivity of Fluids with Nanoparticles, USA, *ASME, FED 231/MD*, *66* (1995), Jan., pp. 99-105

[8] Buongiorno, J., Convective Transport in Nanofluids, *Journal of Heat Transfer*, *128* (2006), 3, pp. 240-250
[9] Eastman, J. A., Anomalously Increased Efffective Thermal Conductivity of Ethylene Glycol-Based Nanofluids Containing Copper Nanoparticles, *Applied Physics Letters*, *78* (2001), 6, pp. 718-720
[10] Turkyilmazoglu, M., Exact Analytical Solutions for Heat and Mass Transfer of MHD Slip Flow in Nanofluids, *Chemical Engineering Science*, *84* (2012), Dec., pp. 182-187
[11] Sheikholeslami, M., The MHD Free Convection of Al_2O_3-Water Nanofluid Considering Thermal Radiation: A Numerical Study, *International Journal of Heat and Mass Transfer*, *96* (2016), May, pp. 513-524
[12] Hsiao, K. L., Stagnation Electrical, MHD Nanofluid Mixed Convection with Slip Boundary on a Stretching Sheet, *Applied Thermal Engineering*, *98* (2016), Apr., pp. 850-861
[13] Hayat, T., *et al*., Modelling Tangent Hyperbolic Nanoliquid-Flow with Heat and Mass Flux Conditions, *The European Physical Journal Plus*, *132* (2017), Mar., 112
[14] Zhang, C., *et al*., The MHD Flow and Radiation Heat Transfer of Nanofluids in Porous Media with Variable Surface Heat Flux and Chemical Reaction, *Applied Mathematical Modelling*, *39* (2015), 1, pp. 165-181
[15] Hayat, T., *et al*., The 3-D Flow of Powell-Eyring Nanofluid with Heat and Mass Flux Boundary Conditions, *Chines Physics B*, *25* (2016), 7, 074701
[16] Malvandi, A., *et al*., Laminar Filmwise Condensation of Nanofluids over a Vertical Plate Considering Nanoparticles Migration, *Applied Thermal Engineeing*, *100* (2016), May, pp. 979-986
[17] Hayat, T., *et al*., The 3-D Mixed Convection Flow of Sisko Nanoliquid, *International Journal of Mechanical Sciences*, *133* (2017), Nov., pp. 273-282
[18] Hsiao, K. L., To Promote Radiation Electrical MHD Activation Energy Thermal Extrusion Manufacturing System Efficiency by Using Carreau-Nanofluid with Parameters Control Method, *Energy*, *130* (2017), July, pp. 486-499
[19] Hayat, T., *et al*., The MHD flow of Powell-Eyring Nanofluid over a Non-Linear Stretching Sheet with Variable Thickness, *Results in Physics*, *7* (2017), Dec., pp. 189-196
[20] Hsiao, K. L., Micropolar Nanofluid-Flow with MHD and Viscous Dissipation Effects Towards a Stretching Sheet with Multimedia Feature, *International Journal of Heat and Mass Transfer*, *112* (2017), Sept., pp. 983-990
[21] Hayat, T., *et al*., Flow of Magneto Williamson Nanoliquid Towards Stretching Sheet with Variable Thickness and Double Stratification, *Radiation Physics and Chemistry*, *152* (2018), Nov., pp. 151-157
[22] Ullah, I., *et al*., Thermally Radiated Squeezed Flow of Magneto-Nanofluid between Two Parallel Disks with Chemical Reaction, *Journal of Thermal Analysis and Calorimetry*, *135* (2018), July, pp. 1021-1030
[23] Andersson, H. I., Valnes, O. A., Flow of a Heated Ferrofluid over a Stretching Sheet in the Presence of a Magnetic Dipole, *Acta Mechanica*, *128* (1998), Mar., pp. 39-47
[24] Selimefendigil, *et al*., Effect of Rotating Cylender in Forced Convection of Ferrofluid over a Backward Facing Step, *International Journal of Heat and Mass Transfer*, *372* (2014), Apr., pp. 122-133
[25] Mustafa, M., *et al*., Rotating Flow of Magnetite-Water Nanofluid over a Stretching Surface Inspired by Non-Linear Thermal Radiation, *Plos One*, *11* (2016), Feb., pp. e0149304
[26] Hayat T., *et al*., Partial Slip Effect in Flow of Magnetite-Fe_3O_3 Nanoparticles between Rotating Stretchable Disk, *Journal of Magnetism and Magnetic Materials*, *413* (2016), Sept., pp. 39-48
[27] Hayat, T., *et al*., Magnetohydrodynamic (MHD) 3-D flow of Second Grade Nanofluid by a Convectively Heated Exponentially Stretching Surface, *Journal of Molecular Liquids*, *220* (2016), Aug., pp. 1004-1012
[28] Sheikholeslami, M., Hayat T., Alsaedi, A., Numerical Simulation of Nanofluid Forced Convection Heat Transfer Improvement in Existence of Magnetic Field Using Lattice Boltzmann Method, *International Journal of Heat and Mass Transfer*, *108* (2017), Part B, pp. 1870-1883
[29] Liao, S. J., On the Homotopy Analysis Method for Non-Linear Problems, *Applied Mathematics and Computation*, *147* (2004), 2, pp. 499-513
[30] Hayat, T., *et al*., Joule Heating Effects in MHD Flow of Burgers' Fluid, *Heat Transfer Research*, *47* (2016), 12, pp. 1083-1092
[31] Abbasbandy, S., *et al*., Numerical and Analytical Solutions for Falkner-Skan Flow of MHD Oldroyd-B Fluid, *International Journal of Numerical Methods Heat Fluid-Flow*, *24* (2014), 2, pp. 390-401
[32] Hayat, T., *et al*., On Comparison of Series and Numerical Solutions for Flow of Eyring-Powell Fluid with Newtonian Heating and Internal Heat Generation/Absorption, *PloS One*, *10* (2015), Sept., pp. e0129613
[33] Zhn, J., *et al*., Effects of Second order Velocity Slip and Nanoparticles Migration on Flow of Buongiorno Nanofluid, *Applied Mathematical Letters*, *52* (2016), Feb., pp. 183-191
[34] Turkyilmazoglu, M., An Effective Approach for Evaluation of the Optimal Convergence Control Parameter in the Homotopy Analysis Method, *Filomat*, *30* (2016), 6, pp. 1633-1650

[35] Hayat, T., *et al*., Radiative 3-D Flow with Soret and Dufour Effects, *International Journal of Mechanical Sciences*, *133* (2017), Nov., pp. 829-837
[36] Hayat, T., *et al*., Influence of Thermal Radiation and Joule Heating in the Eyring-Powell Fluid-Flow with the Soret and Dufour Effects, *Journal of Applied Mechanics and Technical Physics*, *57* (2016), Feb., pp. 1051-1060
[37] Hayat, T., *et al*., A Revised Model for Stretched Flow of Third Grade Fluid Subject to Magneto Nanoparticles and Convective Condition, *Journal of Molecular Liquids*, *230* (2017), Mar., pp. 608-615
[38] Farooq, A., *et al*., Soret and Dufour Effects on 3-D Oldroyd-B fluid, *Physica A*, *503* (2018), Aug., pp. 345-354
[39] Hayat, T., *et al*., Radiative Flow of Carreau Liquid in Presence of Newtonian Heating and Chemical Reaction, *Results Physics*, *7* (2017), Jan., pp. 715-722
[40] Hayat, T., *et al*., The MHD Mixed Convection Flow of Third Grade Liquid Subject to Non-Linear Thermal Radiation and Convective Condition, *Results Physics*, *7* (2017), Aug., pp. 2804-2811
[41] Rashidi, M. M., *et al*., Mixed Convection Boundary-Layer Flow of Micro Polar Fluid Towards a Heated Shrinking Sheet by Homotopy Analysis Method, *Thermal Science*, *20* (2016), 1, pp. 21-34
[42] Ahmad, S., *et al*., Impact of Arrhenius Activation Energy in Viscoelastic Nanomaterial Flow Subject to Binary Chemical Reaction and Non-Linear Mixed Convection, *Thermal Science*, *24* (2018), 1B, pp. 1143-1155
[43] Zaigham, Z., *et al*., Cross Diffusion and Exponential Space Dependent Heat Source Impacts in Radiated 3-D (3D) Flow of Casson Fluid by Heated Surface, *Results in Physics*, *8* (2018), Mar., pp. 1275-1282
[44] Hsiao, K. L., Combined Electrical MHD Heat Transfer Thermal Extrusion System Using Maxwell Fluid with Radiative and Viscous Dissipation Effects, *Applied Thermal Engineering*, *112* (2017), Feb., pp. 1281-1288
[45] Hayat, T., *et al*., Simultaneous Effects of Non-Linear Mixed Convection and Radiative Flow Due to Riga-Plate with Double Stratification, *Journal of Heat Transfer*, *140* (2018), 10, 102008
[46] Reddy C, S., *et al*., The MHD Flow and Heat Transfer Characteristics of Williamson Nanofluid over a Stretching Sheet with Variable Thickness and Variable Thermal Conductivity, *Transactions of A. Razmadze Mathematical Institute*, *171* (2017), 2, pp. 195-211
[47] Hayat, T., *et al*., Flow of Chemically Reactive Magneto Cross Nanoliquid with Temperature-Dependent Conductivity, *Applied Nanosciences*, *8* (2018), May, pp. 1453-1460

Paper submitted: January 21, 2018
Paper revised: July 26, 2018
Paper accepted: August 10, 2018